bioRxiv preprint doi: https://doi.org/10.1101/2021.11.04.466704; this version posted November 5, 2021. The copyright holder for this preprint (which was not certified by peer review) is the author/funder, who has granted bioRxiv a license to display the preprint in perpetuity. It is made available under aCC-BY-NC-ND 4.0 International license.

Chitin and cuticle proteins form the cuticular layer in spinning duct of silk-spinning arthropods

Xin Wang[1, 2, ‡], Xiaoqian Xie[1, 2, ‡], Kang Xie[1, 2], Qingsong Liu[1, 2], Yi Li[1, 2], Xiaoyin Tan[1, 2], Haonan Dong[1, 2], Xinning Li[1, 2], Zhaoming Dong[1, 2], Qingyou Xia[1, 2], Ping Zhao[1, 2, *]

[1] State Key Laboratory of Silkworm Genome Biology, Southwest University, Chongqing 400716, China; Biological Science Research Center, Southwest University, Chongqing 400716, China.

[2] Chongqing Engineering and Technology Research Center for Novel Silk Materials, Southwest University, Chongqing 400716, China; Chongqing Key Laboratory of Sericulture, Southwest University, Chongqing 400716, China.

* Corresponding author: Ping Zhao. Address: No. 2 Tiansheng Road, Beibei District, Chongqing, 400716, China. Tel: +86 23 68250885. E-mail: zhaop@swu.edu.cn.

‡ Contributed equally.

bioRxiv preprint doi: https://doi.org/10.1101/2021.11.04.466704; this version posted November 5, 2021. The copyright holder for this preprint (which was not certified by peer review) is the author/funder, who has granted bioRxiv a license to display the preprint in perpetuity. It is made available under aCC-BY-NC-ND 4.0 International license.

ABSTRACT

Chitin is found in the exoskeleton and peritrophic matrix of arthropods, but recent studies have also identified chitin in the spinning duct of silk-spinning arthropods. Here, we report the presence and function of chitin and cuticle proteins ASSCP1 and ASSCP2 in the spinning duct of silkworms. We show that chitin and these proteins are co-located in the cuticular layer of the spinning duct. Ultrastructural analysis indicates that the cuticular layer has a multilayer structure by layered stacking of the chitin laminae. After knocking down ASSCP1 and ASSCP2, the fine structure of this layer was disrupted, which had negative impacts on the mechanical properties of silk. This work clarifies the function of chitin in the spinning duct of silk-spinning arthropods. Chitin and cuticle proteins are the main components of the hard and rigid cuticular layer, providing the shearing stress during silk fibrillogenesis and regulating the final mechanical properties of silk.

KEYWORDS

Chitin; Cuticle protein; Cuticular layer; Mechanical properties; Silk fibrillogenesis

bioRxiv preprint doi: https://doi.org/10.1101/2021.11.04.466704; this version posted November 5, 2021. The copyright holder for this preprint (which was not certified by peer review) is the author/funder, who has granted bioRxiv a license to display the preprint in perpetuity. It is made available under aCC-BY-NC-ND 4.0 International license.

INTRODUCTION

Arthropods, which are characterized by their exoskeleton, segmental body, and paired joint appendages, are the most successful and diverse animal species in our living world. Arthropods have significant capabilities for rapid adaptation and colonization in a variety of environments, such as the ground, ocean, and sky. The success of arthropods can be attributed to their unique characteristics. One of the features is the presence of the exoskeleton, which provides extensive protection from various harms, including mechanical damage, radiation, desiccation, and invasion by pathogenic microorganisms.

The exoskeleton is comprised of chitin and chitin-binding proteins (such as different types of cuticle proteins) (Liu, Zhang, & Zhu, 2019). Chitin is a linear polymer of the amino sugar N-acetyl-D-glucosamine, which can be easily found in the cuticle of the exoskeleton and the peritrophic matrix of the midgut in arthropods. It has been reported that the chitin content of the exuvial dry mass may be as high as 40% (Kramer, Hopkins, & Schaefer, 1995). The chitin content in the exoskeleton affects egg hatching (Zhu, Arakane, Beeman, Kramer, & Muthukrishnan, 2008), molting at various stages (He et al., 2013; Pesch, Riedel, Patil, Loch, & Behr, 2016), wing development (Chen, Yang, Tang, Yang, & Jin, 2017; Noh, Muthukrishnan, Kramer, & Arakane, 2018), and survival of arthropods (He et al., 2013; Su et al., 2016). In the peritrophic matrix, chitin is related to the permeability of small solutes and water (Agrawal et al., 2014), digestion of food (Liu et al., 2012), and size of the peritrophic matrix (Liu et al.,

bioRxiv preprint doi: https://doi.org/10.1101/2021.11.04.466704; this version posted November 5, 2021. The copyright holder for this preprint (which was not certified by peer review) is the author/funder, who has granted bioRxiv a license to display the preprint in perpetuity. It is made available under aCC-BY-NC-ND 4.0 International license.

2012).

In addition to being present in the exoskeleton and peritrophic matrix, chitin is also found in the spinning duct of some silk-spinning arthropods, such as silkworms (Davies, Knight, & Vollrath, 2013), spiders (Davies et al., 2013), and caddisworms (Ashton & Stewart, 2019). The spinning duct of silk-spinning arthropods is the place where solid silk fiber is formed. It has been generally accepted that silk proteins undergo a gel-sol transition accompanied by physical and biochemical changes, such as pH (Askarieh et al., 2010; Hagn et al., 2010), metal ions (Wang, Li, Liu, Chen, et al., 2017; Wang, Li, et al., 2015; Wang, Zhao, et al., 2015; Zhou, Chen, Shao, Huang, & Knight, 2005), and shearing forces (Eisoldt, Hardy, Heim, & Scheibel, 2010; Holland, Urbach, & Blair, 2012; Rammensee, Slotta, Scheibel, & Bausch, 2008) in the spinning duct. Despite being an essential component of the spinning duct, the roles that chitin plays in this process remain unclear.

To understand the functions of the spinning duct in silk fibrillogenesis, RNA-seq and proteomics techniques have been introduced (Chang et al., 2015; Wang, Li, Liu, Xia, & Zhao, 2017; Wang et al., 2016; Yi et al., 2013). A large number of cuticle proteins have been identified in the silkworm spinning duct. Most of these proteins are predicted to have the chitin-binding domain (Wang, Li, Liu, Xia, et al., 2017; Yi et al., 2013). In our previous studies, we identified two cuticle proteins named ASSCP1 and ASSCP2 that are highly and specifically expressed in the spinning duct of silkworm (Wang et al., 2016; Yi et

bioRxiv preprint doi: https://doi.org/10.1101/2021.11.04.466704; this version posted November 5, 2021. The copyright holder for this preprint (which was not certified by peer review) is the author/funder, who has granted bioRxiv a license to display the preprint in perpetuity. It is made available under aCC-BY-NC-ND 4.0 International license.

al., 2013). These proteins belong to the RR-2 family and possess the typical chitin-binding domain (Yi et al., 2013), which makes them the perfect targets to study the function of chitin in the spinning duct and the relationship between chitin and cuticle proteins.

In the present study, we aimed to investigate the functions of cuticle proteins and chitin in silk fibrillogenesis, as well as the expression pattern, localization, and chitin-binding activity of these proteins.

MATERIALS AND METHODS

Silkworms

Silkworms at different developmental stages were obtained from the Biological Science Research Center (Southwest University, China). Silk glands were dissected from the silkworm and divided into five parts (ASG, AMSG, MMSG, PMSG, and PSG) carefully according to their distinct morphology. After rinsing with sterilized water, all the samples were frozen rapidly in liquid nitrogen and stored at -80 ºC.

Chitin content assay

Chitin content of the different parts of the silk gland was assayed according to the method of Zhang and Zhu (2006). Briefly, 0.1 g sample was homogenized with distilled water and centrifuged at 1800 ×*g* for 15 min at 25 ºC. The pellet was resuspended in 3% SDS. Next, the sample was incubated at 100 ºC for 15 min and centrifuged for 10 min. The resulting pellet was washed with distilled water, resuspended in 14 M KOH, and incubated at 130 ºC for 1 h to deacetylate

bioRxiv preprint doi: https://doi.org/10.1101/2021.11.04.466704; this version posted November 5, 2021. The copyright holder for this preprint (which was not certified by peer review) is the author/funder, who has granted bioRxiv a license to display the preprint in perpetuity. It is made available under aCC-BY-NC-ND 4.0 International license.

chitin. The deacetylated sample was cooled on ice for 5 min and resuspended in ice-cold 75% ethanol. After being incubated on ice for 15 min, 35 µL of Celite 545 suspension was added to each sample. The samples were centrifuged at 1,800 ×*g* for 15 min at 4 ºC. The resulting pellet (insoluble chitosan) was washed with 40% cold ethanol and resuspended in distilled water. These samples were mixed with 10% $NaNO_2$ and 10% $KHSO_4$. After gentle shaking, samples were incubated at 25 ºC for 15 min to depolymerize the chitosan and deaminate the glucosamine residues from the chitosan. Samples were then centrifuged at 1,800 ×*g* for 15 min at 4 ºC and the supernatant was collected. After the addition of 12.5% $NH_4SO_3NH_2$, the mixtures were vigorously shaken for 5 min at 25 ºC. Next, 0.5% freshly prepared 3-methyl-2-benzothiazolone hydrazine hydrochloride hydrate (MBTH) was added to each sample. The samples were incubated at 100 ºC for 5 min. After cooling for 10 min at 25 ºC, 20 µL of 0.83% $FeCl_3 \cdot 6H_2O$ solution was added, and the solution was thoroughly mixed. The cooled samples were placed on a 96-well microplate to determine the absorbance at 650 nm. Commercial glucosamine was used in a standard curve to determine the chitin content. All the chemicals and reagents were purchased from Sigma-Aldrich (USA).

Western blotting

Proteins were extracted using 8 M urea with 30 mM DL-dithiothreitol (DTT). Protein concentration was determined using the method of Bradford. Samples (containing 20 µg of total protein) were mixed with loading buffer and separated

bioRxiv preprint doi: https://doi.org/10.1101/2021.11.04.466704; this version posted November 5, 2021. The copyright holder for this preprint (which was not certified by peer review) is the author/funder, who has granted bioRxiv a license to display the preprint in perpetuity. It is made available under aCC-BY-NC-ND 4.0 International license.

on 12 % SDS-PAGE gels and transferred to PVDF membranes (Roche, Switzerland). After blocking with Tris-buffered saline with 0.1% Tween 20 and 5 % nonfat dry milk, the membrane was incubated with an affinity-purified specific antibody (1:10,000) and goat peroxidase-conjugated antirabbit IgG (1:20,000, Sigma-Aldrich, USA), for 2 h at 25 ºC. Immunoreactive protein signals were visualized using stable peroxide solution and luminol/enhancer solution (Millipore, USA). Silkworm α-tubulin protein was used as an internal control.

Immunofluorescence

ASG samples were dissected on ice and fixed in 4% paraformaldehyde for 1 h at 25 ºC. Next, samples were frozen in Tissue-Tek (Sakura, Japan) at -80 ºC. Sections of 7 μm in thickness were cut by freezing microtome (Leica, Germany). The sections were used for immunofluorescence according to a previously described method (Wang, Zhao, et al., 2015). Chitin in the ASG was labeled using FITC conjugated wheat germ agglutinin (FITC-WGA, Sigma-Aldrich, USA).

Expression and purification of recombinant protein

A fragment containing the RR-2 consensus sequence of *ASSCP1* (Fig. S1) was cloned and inserted into an expression vector (pET-28a). The primers used for PCR amplification are listed in Table S1. The vector was transformed into *Escherichia coli* BL21(DE3). The recombinant protein (ASSCP1-R) was induced by adding isopropyl β-D-1-thiogalactopyranoside (IPTG) into the LB

bioRxiv preprint doi: https://doi.org/10.1101/2021.11.04.466704; this version posted November 5, 2021. The copyright holder for this preprint (which was not certified by peer review) is the author/funder, who has granted bioRxiv a license to display the preprint in perpetuity. It is made available under aCC-BY-NC-ND 4.0 International license.

media and purified by Ni-NTA affinity chromatography (Qiagen, USA). The full length of ASSCP2 protein (ASSCP2-R) was also expressed and purified according to the same protocols. Then, the rabbit polyclonal antibodies against ASSCP1 or ASSCP2 were produced and purified commercially by Zoonbio Biotech (China).

Preparation of chitin-binding proteins in ASG

ASG samples were homogenized in 20 mM PBS buffer (pH 7.4) with 15 mM NaCl and centrifuged at 12,000 × *g* for 20 min at 4 ºC. Proteins were then extracted from the pellets in 20 mM PBS buffer (pH 7.4) containing 2 % SDS. The mixture was vortexed at 25 ºC for 2 h, centrifuged at 12,000 ×*g* for 20 min at 25 ºC, and the supernatant was collected. Next, 1 M KCl was added into each sample to remove most of the SDS. The supernatant was collected by centrifugation (12,000 ×*g*, 10 min, 4 ºC) and diluted 20-fold with 1 mM HEPES (pH 7.4). To remove residual SDS, an ultrafiltration tube (MWCO 10 kDa, Millipore) was used by adding 1 mM HEPES (pH 7.4) into the solution and centrifuging at 4,000 ×*g* for 20 min at 4 ºC repeatedly until the SDS concentration was sufficiently low (<0.001%). The concentration of SDS in the samples was determined according to a previously described method (Arand, Friedberg, & Oesch, 1992).

Chitin and cellulose binding assay

Chitin and cellulose binding assay was performed as previously described (Tang, Liang, Zhan, Xiang, & He, 2010). Briefly, chitin (New England BioLabs,

bioRxiv preprint doi: https://doi.org/10.1101/2021.11.04.466704; this version posted November 5, 2021. The copyright holder for this preprint (which was not certified by peer review) is the author/funder, who has granted bioRxiv a license to display the preprint in perpetuity. It is made available under aCC-BY-NC-ND 4.0 International license.

UK) and cellulose (Sigma-Aldrich, USA) beads were equilibrated in 20 mM HEPES (pH 7.4) containing 15 mM NaCl. A total of 3 mL solution (containing 3 mg ASG proteins or recombinant proteins) was mixed with 1 mL equilibrated chitin or cellulose beads for 3 h at 4 ºC with gentle shaking. Next, the slurries were packed into a column and washed with 20 mM HEPES (pH 7.4) and 1 M NaCl five times. The flow-through component and the washing eluate are referred to as F and W fractions, respectively. The bound proteins were eluted with 20 mM HEPES (pH 7.4) containing 15 mM NaCl and 8 M urea. The resulting eluate is referred to as E fraction. All these fractions were collected and used for subsequent SDS-PAGE and western blotting analyses.

Transgenic vector construction and transgenic silkworm isolation

To study the physiological functions of ASSCP1 and ASSCP2, we constructed two transgenic vectors in which the dsRNA of *ASSCP1* or *ASSCP2* gene was controlled by a spinning duct specific promoter (*BmCP231*). The fragments of the dsRNA of the *ASSCP1* or *ASSCP2* gene were synthesized by Sangon Biotech Company (China) according to the CDS sequences of these genes. The sequences can be found in Table S2. In these vectors, the *RFP* gene or *GFP* gene acted as the marker gene that was driven by the *3×P3* promoter and expressed in the compound eyes and nervous tissues of *B. mori* (Fig. S5). All the primers used are listed in Table S1. After purification, each vector was microinjected into silkworm eggs. The generation of non-diapause embryos, microinjection, and screening of transgenic silkworms were

bioRxiv preprint doi: https://doi.org/10.1101/2021.11.04.466704; this version posted November 5, 2021. The copyright holder for this preprint (which was not certified by peer review) is the author/funder, who has granted bioRxiv a license to display the preprint in perpetuity. It is made available under aCC-BY-NC-ND 4.0 International license.

189 performed as previously described (Wang, Zhao, et al., 2015). The transgenic
190 silkworm line was named *ASSCP1*$^{-}$ and *ASSCP2*$^{-}$, respectively. By cross-
191 breeding, we obtained the transgenic line (ASSCP1^{-}/ASSCP2^{-}) that both
192 ASSCP1 and ASSCP2 were knocked down. The economic trait (cocoon shell
193 ratio) of transgenic silkworm lines was assessed by weighing the cocoon and
194 the pupae. Total proteins from ASGs at the 4th molting, 5th instar, and spinning
195 stages were extracted, and western blotting was used to determine whether the
196 expressions of these two cuticle proteins were successfully knocked down in
197 these developmental stages. Chitin content assay was also performed.

198 **Morphological analysis**

199 Morphological analysis of ASG was performed using an EVOS FL Auto
200 Microscope system (Life Technology, USA). All sections of ASG were observed
201 under a confocal microscope (Olympus, Japan). The surface of the cocoon and
202 all the fibers were observed using scanning electron microscopy (SEM, Hitachi,
203 Japan) at an acceleration voltage of 5 kV and a polarizing optical microscope
204 (Leica, Germany). For transmission electron microscope (TEM) observations,
205 fresh ASG was dissected, cut into 1 mm^3 section, and fixed in ice-cold 2.5 %
206 glutaraldehyde solution (Sigma-Aldrich, USA) for 24 h. ASG sections were then
207 dehydrated in an ethanol series from 50% to 90%, embedded in Spurr resin
208 (Spi-Chem, USA), cured, and cut into 70-nm sections. Sections were stained
209 using 3% uranyl acetate-lead citrate (Spi-Chem, USA). A TEM (JEM1230, JEOL,
210 Japan) was used to capture the images. For the immunoelectron microscopy,

bioRxiv preprint doi: https://doi.org/10.1101/2021.11.04.466704; this version posted November 5, 2021. The copyright holder for this preprint (which was not certified by peer review) is the author/funder, who has granted bioRxiv a license to display the preprint in perpetuity. It is made available under aCC-BY-NC-ND 4.0 International license.

211 resin blocks were cut to 70 nm thin and the tissues were fished out onto the
212 150 meshes nickel grids with formvar film. After rinsing, the tissues were
213 blocked for 30 min in a TBS solution containing 1% BSA. Then, the nickel grids
214 were incubated in the ASSCP1 antibody (1:30) diluted in TBS solution
215 containing 1% BSA. After rinsing on TBS solution 3 times, the nickel grids were
216 incubated in the secondary antibody solution and washed by TBS solution. 2%
217 uranium acetate saturated alcohol solution was used for staining the nickel
218 grids. After that, the nickel grids are observed under the TEM. The 10 nm black
219 golden particles are positive signals of the target proteins.

220 **FTIR analysis of silk fibers**

221 The degumming process, FTIR analysis, and peak deconvolution were
222 performed according to the previous literatures (Peng et al., 2019; Wang, Li,
223 Liu, Chen, et al., 2017). Briefly, five cocoons from each silkworm line were
224 chosen randomly and degummed by boiling in two 30 min rounds using 0.5%
225 (w/v) $NaHCO_3$ solution. The degummed silk fibers were washed with distilled
226 water and allowed to air dry at room temperature. Then, infrared spectroscopy
227 in attenuated total internal reflection mode was performed on these fibers using
228 a Thermo Scientific (USA) Nicolet iN10 with a Slide-On ATR objective lens. The
229 spectra were recorded in the 650−4000 cm^{-1} range at a resolution of 8 cm^{-1}
230 with 256 scans for each measurement. The applied ATR current pressure was
231 set to 75. OMNIC 9 software (ThermoScientific, USA) was used to collect and
232 process the spectral data. Baseline correction, deconvolution of amide I bands,

bioRxiv preprint doi: https://doi.org/10.1101/2021.11.04.466704; this version posted November 5, 2021. The copyright holder for this preprint (which was not certified by peer review) is the author/funder, who has granted bioRxiv a license to display the preprint in perpetuity. It is made available under aCC-BY-NC-ND 4.0 International license.

and peak fitting were performed using OMNIC 9 software (ThermoScientific) and PeakFit software (Seasolve, version 4.12, USA). The content of each secondary structural component is determined by measuring the ratios of areas under the corresponding peaks (Fig. S10).

Mechanical testing of silk fibers

To accurately compare the mechanical properties of silks between each silkworm line, we used the forcible silking method to obtain single silk fibers. Since the environmental conditions have a great influence on the mechanical properties of silks, it is easier to precisely control these conditions by forcible silking. Briefly, spinning silkworms were divided into weight-matched groups. The single silk was grasped and reeled artificially from the silkworm spinneret using a device developed by Khan et al. (Khan et al., 2008) and modified by ourselves. We attempted to obtain silk fibers at 60 rpm/min for more than 10 min. The single silk fiber was cut to a length of 10 mm. The diameter of each silk fiber was measured across two brins under optical microscopy (Zeiss, Germany). The fiber cross-section area was calculated by using the diameter. It should be noted that the cross-sectional shape of silk is approximately elliptical rather than circular, so the cross-sectional area of silk was overestimated in the calculation. Tensile tests were performed on a dynamic mechanical analyzer Q800 (DMA, TA Universal Analysis, USA) at 25 °C and 60% humidity. The stretching speed was set to 1 mm/min. Raw data were collected and analyzed using the TA Universal Analysis software. Subsequently, the data

bioRxiv preprint doi: https://doi.org/10.1101/2021.11.04.466704; this version posted November 5, 2021. The copyright holder for this preprint (which was not certified by peer review) is the author/funder, who has granted bioRxiv a license to display the preprint in perpetuity. It is made available under aCC-BY-NC-ND 4.0 International license.

were used to calculate mechanical performance parameters using ORIGIN 8.0 (OriginLab, USA). Since the cross-sectional area of silk was overestimated, the stress of the silk fiber was underestimated accordingly.

RESULTS

ASSCP1 and ASSCP2 are co-located with chitin in the cuticular layer of the silkworm spinning duct

RNA-Seq and proteomics approaches have identified ASSCP1 and ASSCP2 as the silkworm spinning duct specific cuticle proteins, which are predicted to have the chitin-binding domain (Chang et al., 2015; Wang et al., 2016; Yi et al., 2013). If these proteins can bind chitin, they should be co-located with chitin in the same tissue. To test this possibility, western blotting and immunofluorescence were performed (Fig. 1). Anterior silk gland (ASG), spinneret, and Filippi's gland constitute the spinning duct of the silkworm. Because the spinneret and Filippi's gland are both quite small, we used the ASG to perform the experiments. Tissue distributions of ASSCP1 and ASSCP2 revealed that they were only expressed in ASG (Fig. 1A). Furthermore, the localization of these two proteins and chitin were determined using frozen sectioning and immunofluorescence. As shown in Fig. 1B, the green signal was detected in the cuticular layer of ASG, indicating that the chitin is located in this region. The signals from ASSCP1 and ASSCP2 were also detected in the cuticular layer (Fig. 1B), suggesting that both cuticle proteins and chitin are co-located in the cuticular layer of the silkworm spinning duct.

bioRxiv preprint doi: https://doi.org/10.1101/2021.11.04.466704; this version posted November 5, 2021. The copyright holder for this preprint (which was not certified by peer review) is the author/funder, who has granted bioRxiv a license to display the preprint in perpetuity. It is made available under aCC-BY-NC-ND 4.0 International license.

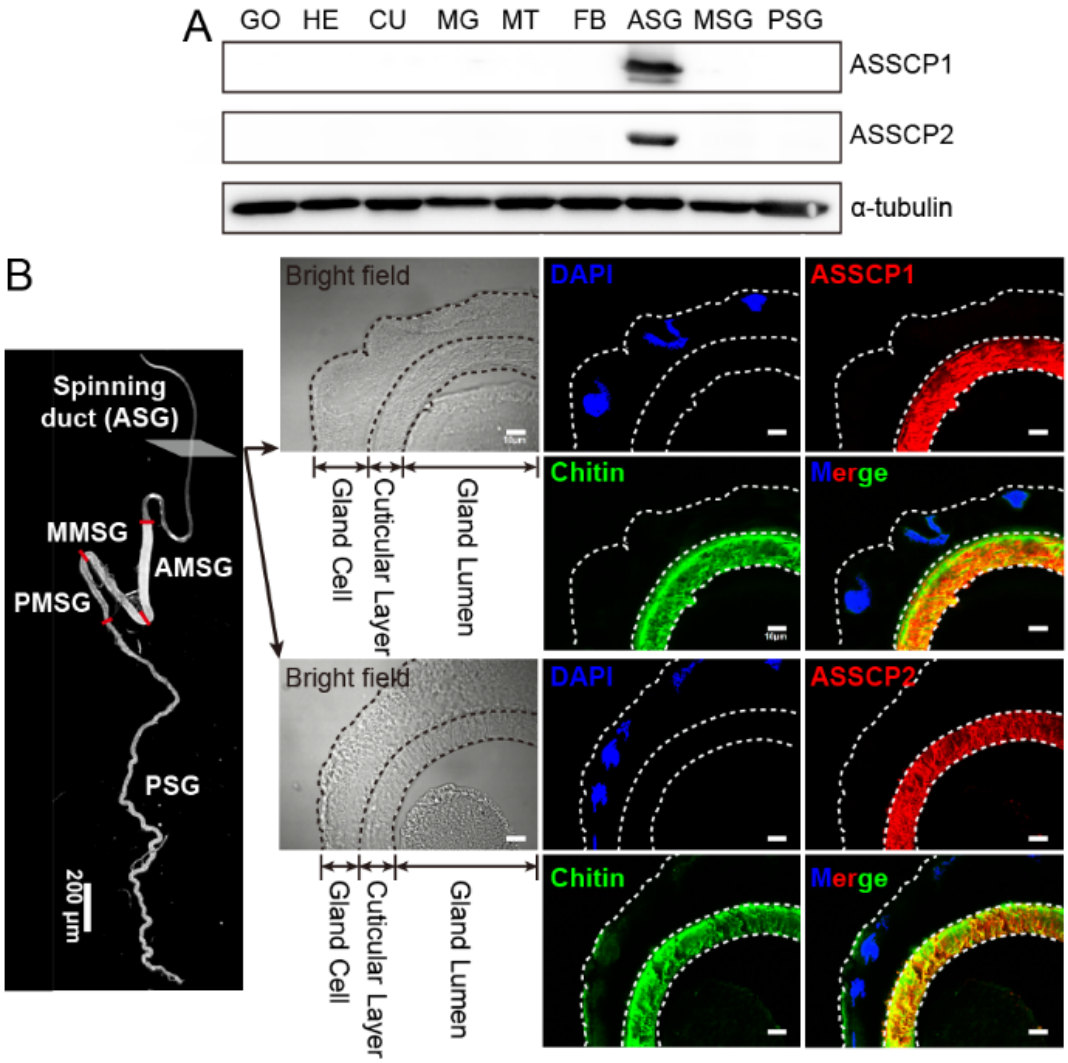

277

278 **Fig. 1** ASSCP1, ASSCP2, and chitin are co-located in the cuticular layer of the silkworm
279 spinning duct. **(A)** Western blotting analysis of ASSCP1 and ASSCP2 in several tissues from
280 the third day of fifth instar silkworm larvae. GO, gonad; HE, head; CU, cuticle; MG, mid-gut; MT,
281 malpighian tubule; FB, fat body; ASG, anterior silk gland; MSG, middle silk gland; PSG,
282 posterior silk gland. **(B)** Localizations of ASSCP1, ASSCP2, and chitin in the ASG from the
283 spinning silkworm. Blue, the signal from the nucleus. Red, signals from ASSCP1 and ASSCP2.
284 Green, the signal from chitin.

285 **ASSCP1 and ASSCP2 are chitin-binding proteins**

286 Although chitin has been found in the spinning duct of silkworms (Davies

bioRxiv preprint doi: https://doi.org/10.1101/2021.11.04.466704; this version posted November 5, 2021. The copyright holder for this preprint (which was not certified by peer review) is the author/funder, who has granted bioRxiv a license to display the preprint in perpetuity. It is made available under aCC-BY-NC-ND 4.0 International license.

et al., 2013), the exact content of chitin in this tissue is still unclear. In the present study, the distributions of chitin in different parts of the silk gland were analyzed. Compared with other parts of the silk gland, the chitin content in ASG is very high (Fig. 2A), whereas the chitin content in MSG and PSG is quite low.

We have found that ASSCP1 and ASSCP2 are co-located with chitin in the cuticular layer of the spinning duct. To investigate whether these proteins could bind chitin, chitin-binding assays were performed using proteins extracted from ASG (AP, Fig. 2B). As shown in Fig. 2B, the protein bands were detected in the elution fractions (E' and E''). Using the ASSCP1 and ASSCP2 specific antibodies, we identified the band in E' and E'' fraction as ASSCP1 and ASSCP2, respectively. These results were further confirmed by matrix assisted laser desorption ionization-time of flight mass spectrometry (MALDI-TOF MS).

Then, we successfully generated and purified a truncated ASSCP1 recombinant protein (ASSCP1-R) and a full-length ASSCP2 recombinant protein (ASSCP2-R) using an *E. coli* expression system (Figs. S1 and S2). The reason why we chose to express the truncated form of ASSCP1 protein is the repeat sequences (eg, SESSSEE, Fig. S1) in the C-terminus prevent expression of the full-length protein.

Chitin and cellulose binding assays were performed using the recombinant proteins. Cellulose was used as a negative control. As shown in Fig. 2C and 2D, the signal was only detected in the elution fraction (E) after recombinant proteins were incubated with chitin beads. In contrast, no signal corresponding

bioRxiv preprint doi: https://doi.org/10.1101/2021.11.04.466704; this version posted November 5, 2021. The copyright holder for this preprint (which was not certified by peer review) is the author/funder, who has granted bioRxiv a license to display the preprint in perpetuity. It is made available under aCC-BY-NC-ND 4.0 International license.

to cellulose binding was observed (Fig. S3). These results suggest that ASSCP1 and ASSCP2 are chitin-binding proteins

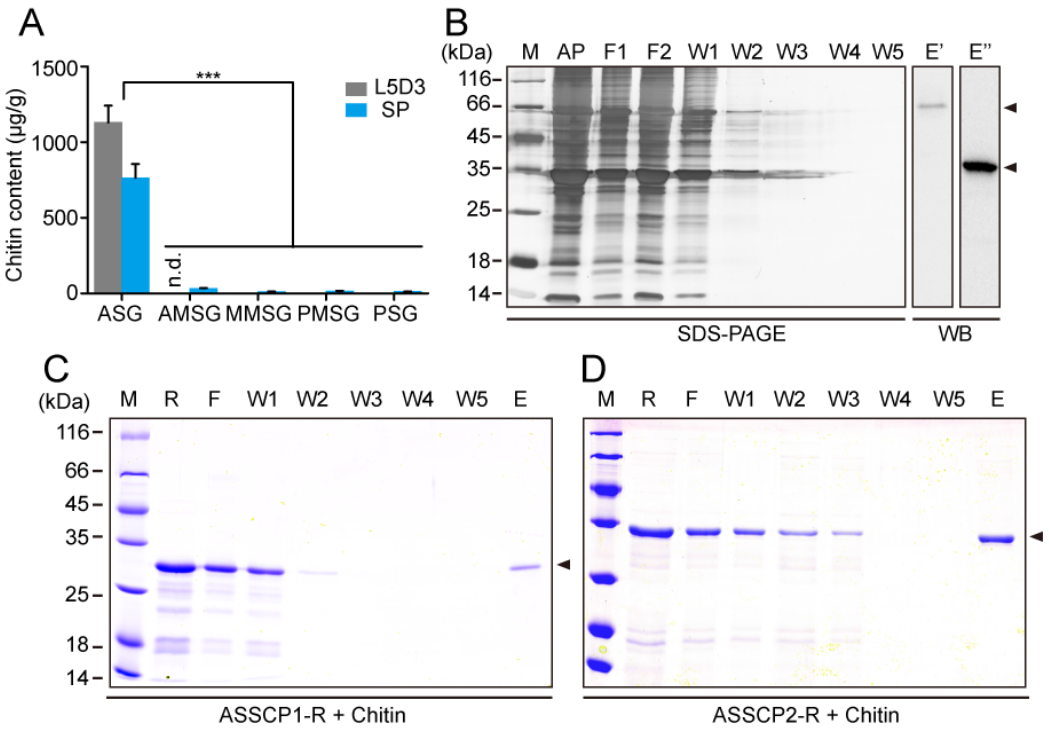

Fig. 2 ASSCP1 and ASSCP2 are chitin-binding proteins. **(A)** Distributions of chitin in different parts of the silkworm silk gland. The decrease in chitin content at the spinning stage was due to the increase in the total weight of ASG. n. d., not detected; L5D3, the sample from the 3rd day of 5th instar larvae; SP, the sample from the spinning larvae; ASG, anterior silk gland; AMSG, the anterior section of middle silk gland; MMSG, the middle section of middle silk gland; PMSG, the posterior section of middle silk gland; PSG, posterior silk gland. ***, *p*-value < 0.001. **(B)** Chitin binding assay of ASG-extracted proteins. ASG proteins were extracted and incubated with commercial chitin beads. Non-specific bound proteins were washed with NaCl and the chitin-binding proteins were eluted with urea. Protein fractions were detected using SDS-PAGE followed by silver nitrate staining and western blotting (WB) with ASSCP1 and ASSCP2 specific antibodies, respectively. Gel condition, 12 % SDS-PAGE; M, protein marker; AP, ASG-extracted

bioRxiv preprint doi: https://doi.org/10.1101/2021.11.04.466704; this version posted November 5, 2021. The copyright holder for this preprint (which was not certified by peer review) is the author/funder, who has granted bioRxiv a license to display the preprint in perpetuity. It is made available under aCC-BY-NC-ND 4.0 International license.

proteins; F1-F2, flow-through fractions; W1-W5, washing fractions; E' and E'', eluted fractions; Arrowhead in E', ASSCP1 protein; Arrowhead in E'', ASSCP2 protein. **(C)** Chitin binding assays of purified recombinant ASSCP1 protein (ASSCP1-R). All fractions were detected using SDS-PAGE followed by Coomassie brilliant blue G-250 staining. M, protein marker; R, recombinant protein; F, flow-through fraction; W1-W5, washing fractions; E, eluted fraction; Arrowhead, ASSCP1-R. **(D)** Chitin binding assays of purified recombinant ASSCP2 protein (ASSCP2-R). Arrowhead, ASSCP2-R.

Cuticle proteins and chitin are periodically present in the silkworm larval stage.

Western blotting was performed to detect the presence of ASSCP1 in different instar larvae. Temporal expression analysis revealed that this protein is expressed only during larval feeding stages (Fig. 3A). The repetitive expression pattern of ASSCP1 during the silkworm feeding-molting transition led us to determine the exact time points of its synthesis and degradation. Thus, we further performed qRT-PCR and SDS-PAGE analysis using the ASG samples from different time points during the fourth molting larvae (Fig. 3B and 3C). It can be seen that the proteins had undergone degradation when larvae began to molt (0 h - 3 h). From 6 h to 12 h after molting, no positive protein bands could be detected but the transcription of the gene was active. The positive signals appeared again in the late molting stage (15 h after molting), indicating that the proteins are re-synthesized.

Immunofluorescence results clearly show that the cuticular layer was

bioRxiv preprint doi: https://doi.org/10.1101/2021.11.04.466704; this version posted November 5, 2021. The copyright holder for this preprint (which was not certified by peer review) is the author/funder, who has granted bioRxiv a license to display the preprint in perpetuity. It is made available under aCC-BY-NC-ND 4.0 International license.

renewed during the IV molting stage (Fig. 3D). Consistent with western blotting results, the positive signal of ASSCP1 (red) and weak signal for chitin (green) were detected in the cuticular layer 3 h after molting. However, the shape of the cuticular layer was irregular, suggesting the degradation process had begun. Six hours after molting, only ASSCP1 could be detected and the cuticular layer was very thin. The cuticular layer was completely degraded 9 h after molting. At the late molting stage, ASSCP1 and chitin signals were both detected in the gland cell and cuticular layer, which indicates that the layer is re-built.

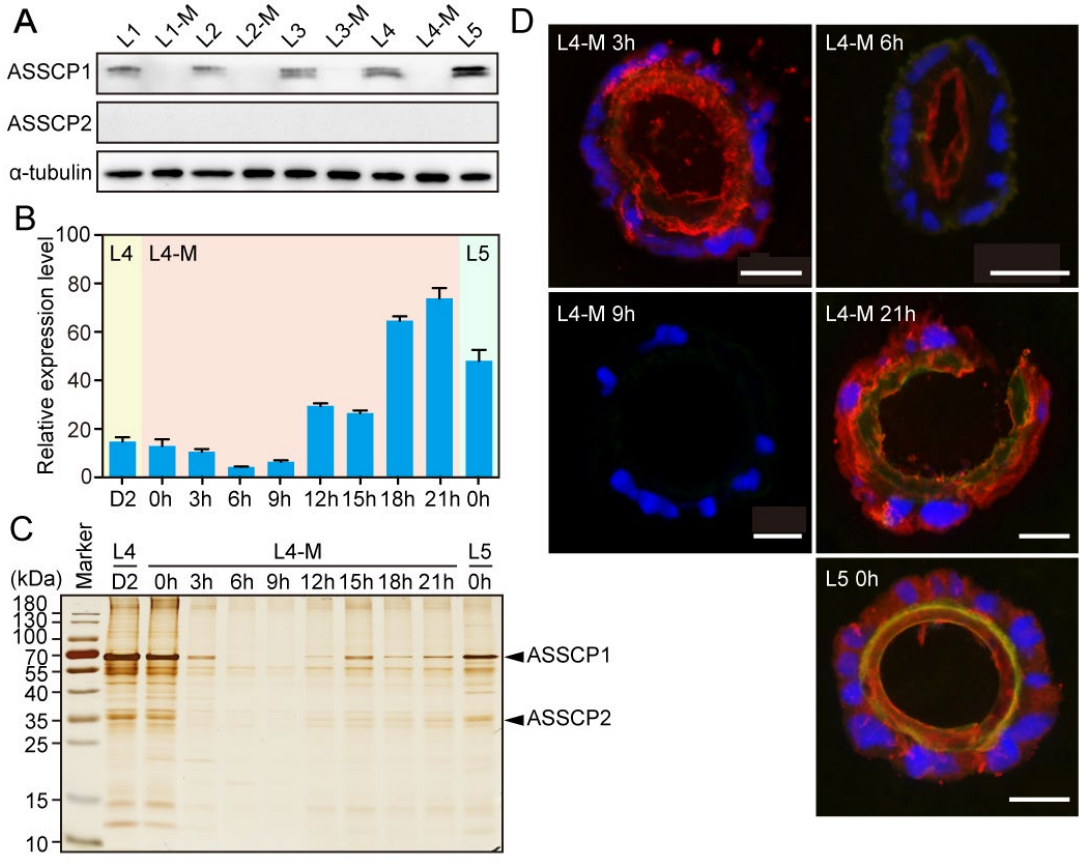

Fig. 3 Cuticle proteins and chitin are periodically expressed. **(A)** Expression profile of ASSCP1 protein in the whole body of silkworm larvae from the first to fifth instar. The expression of ASSCP2 was quite low in these stages, no positive signal could be detected. L1, newly hatched larvae; L1-M, molting larvae on the first instar; L2, feeding larvae on the second instar; L2-M,

bioRxiv preprint doi: https://doi.org/10.1101/2021.11.04.466704; this version posted November 5, 2021. The copyright holder for this preprint (which was not certified by peer review) is the author/funder, who has granted bioRxiv a license to display the preprint in perpetuity. It is made available under aCC-BY-NC-ND 4.0 International license.

358 molting larvae on the second instar; L3, feeding larvae on the third instar; L3-M, molting larvae
359 on the third instar; L4, feeding larvae on the fourth instar; L4-M, molting larvae on the fourth
360 instar; L5, feeding larvae on the fifth instar. **(B)** Expression profile of *ASSCP1* transcripts during
361 the fourth molting stage using qRT-PCR. **(C)** Expression profile of ASSCP1 and ASSCP2
362 proteins during the fourth molting stage using SDS-PAGE, followed by silver nitrate staining. **(d)**
363 Immunofluorescence localization of ASSCP1 in ASG during molting stage in the fourth instar.
364 Blue, nucleus; Green, chitin; Red, ASSCP1 protein; Scale bar, 50 μm.

365 **Cuticle proteins and chitin are constantly present during silk spinning**
366 **and degraded during pupation.**

367 Signals from cuticle proteins and chitin were constantly observed in the
368 cuticular layer during the whole feeding stage of the fifth instar (Fig. S4).
369 Assumed as an essential component of the spinning duct, chitin should be
370 present during the silk spinning process. Thus, we measured the thickness of
371 the cuticular layer during silk spinning to confirm this assumption. Fig. 4A shows
372 that the thickness of the cuticular layer remained unchanged during the silk
373 spinning process. However, the cuticular layer underwent a dramatic
374 degradation during the pupation stage, when silk spinning was complete. We
375 performed morphological analysis of the ASG and found that the ASG
376 morphology remained unchanged during the silk spinning process, but the
377 gland cell contracted and showed obvious apoptotic characteristics during
378 pupation (Fig. 4B). Immunofluorescence analysis revealed that chitin and
379 cuticle proteins were also constantly presented during silk spinning (Fig. 4C).

bioRxiv preprint doi: https://doi.org/10.1101/2021.11.04.466704; this version posted November 5, 2021. The copyright holder for this preprint (which was not certified by peer review) is the author/funder, who has granted bioRxiv a license to display the preprint in perpetuity. It is made available under aCC-BY-NC-ND 4.0 International license.

At the pre-pupation stage, some fissures could be observed on the cuticular layer. At the pupal stage, the cuticular layer was completely degraded and disappeared.

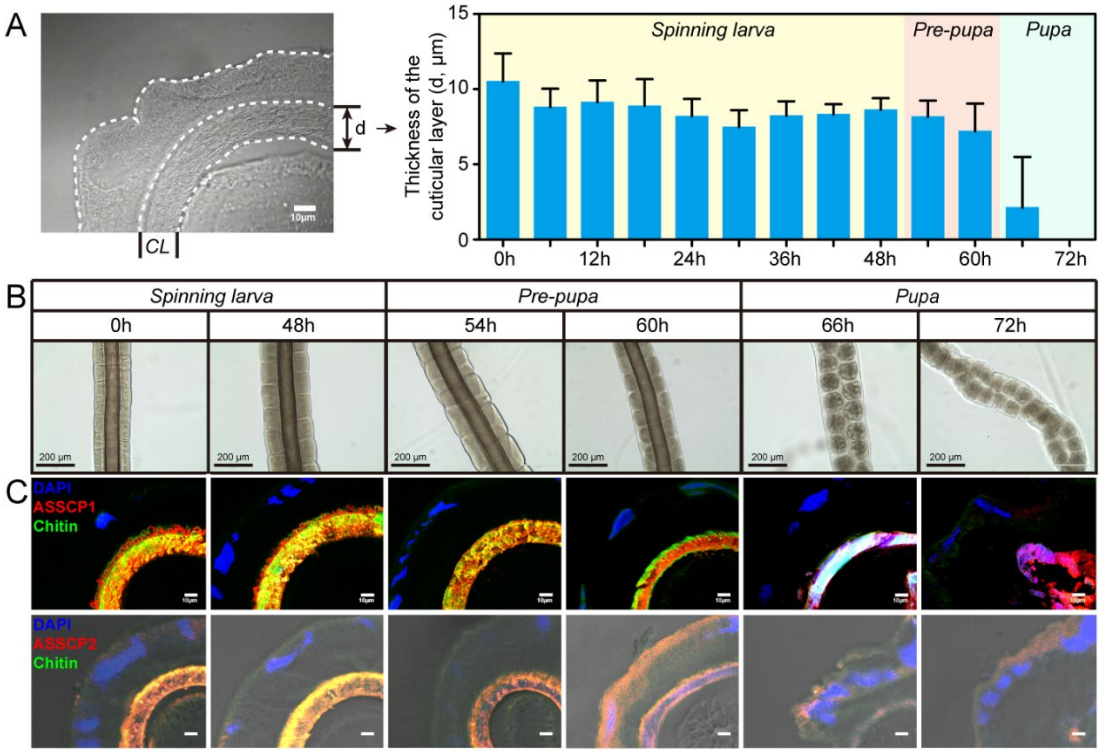

Fig. 4 Cuticle proteins and chitin are constantly present during silk spinning and are degraded during pupation. **(A)** The thickness of the cuticular layer of the spinning duct at different time points during silk spinning and the pupal stages. CL, cuticular layer. Scale bar, 10 μm. **(B)** Morphological analysis of the ASG. Scale bar, 200 μm. **(C)** Immunofluorescence analysis of ASSCP1, ASSCP2, and chitin in ASG. Blue, the nucleus; Red, ASSCP1 and ASSCP2 proteins; Green, chitin. Scale bar, 10 μm.

Fine structure of the cuticular layer in silkworm spinning duct

TEM was used to observe the ultrastructure of the cuticular layer. It can be seen from Fig. 5 that the chitin in the cuticular layer constitutes two-dimensional

bioRxiv preprint doi: https://doi.org/10.1101/2021.11.04.466704; this version posted November 5, 2021. The copyright holder for this preprint (which was not certified by peer review) is the author/funder, who has granted bioRxiv a license to display the preprint in perpetuity. It is made available under aCC-BY-NC-ND 4.0 International license.

horizontal sheets, the laminae. The cross-sectional diagram shows that the laminae had a network structure formed by the crosslink of chitin micro-filaments (Fig. 5A). Gaps (~2 μm in diameter) between the chitin filaments were found, which may facilitate the transportation of water, ions, and other small molecules. From the longitudinal section shown in Fig. 5B, the laminae stacked together to form a multi-layer structure, with an interlayer spacing of ~500 nm. The orientation of the cuticular layer is the same as the direction of silk protein transportation. Furthermore, immunoelectron microscopy (IEM) was introduced to study the localization of cuticle protein in the cuticular layer. The colloidal gold particles in Fig. 5C represent the cuticle protein ASSCP1. It can be seen that after being synthesized, ASSCP1 was stored in the secretory vesicles between the cuticular layer and gland cells, and then further secreted into the cuticular layer (Fig. 5C'). Magnifying the image found that ASSCP1 is mainly distributed in the interspace between laminae (Fig. 5C").

A schematic illustration of the ultrastructure of the cuticular layer is shown in Fig. 5D. The cuticular layer of the silkworm spinning duct is a multilayer structure by layered stacking of the chitin laminae. Inter- or intra- laminar interactions between cuticle proteins and chitin micro-filaments may stabilize the fine structure of the cuticular layer.

bioRxiv preprint doi: https://doi.org/10.1101/2021.11.04.466704; this version posted November 5, 2021. The copyright holder for this preprint (which was not certified by peer review) is the author/funder, who has granted bioRxiv a license to display the preprint in perpetuity. It is made available under aCC-BY-NC-ND 4.0 International license.

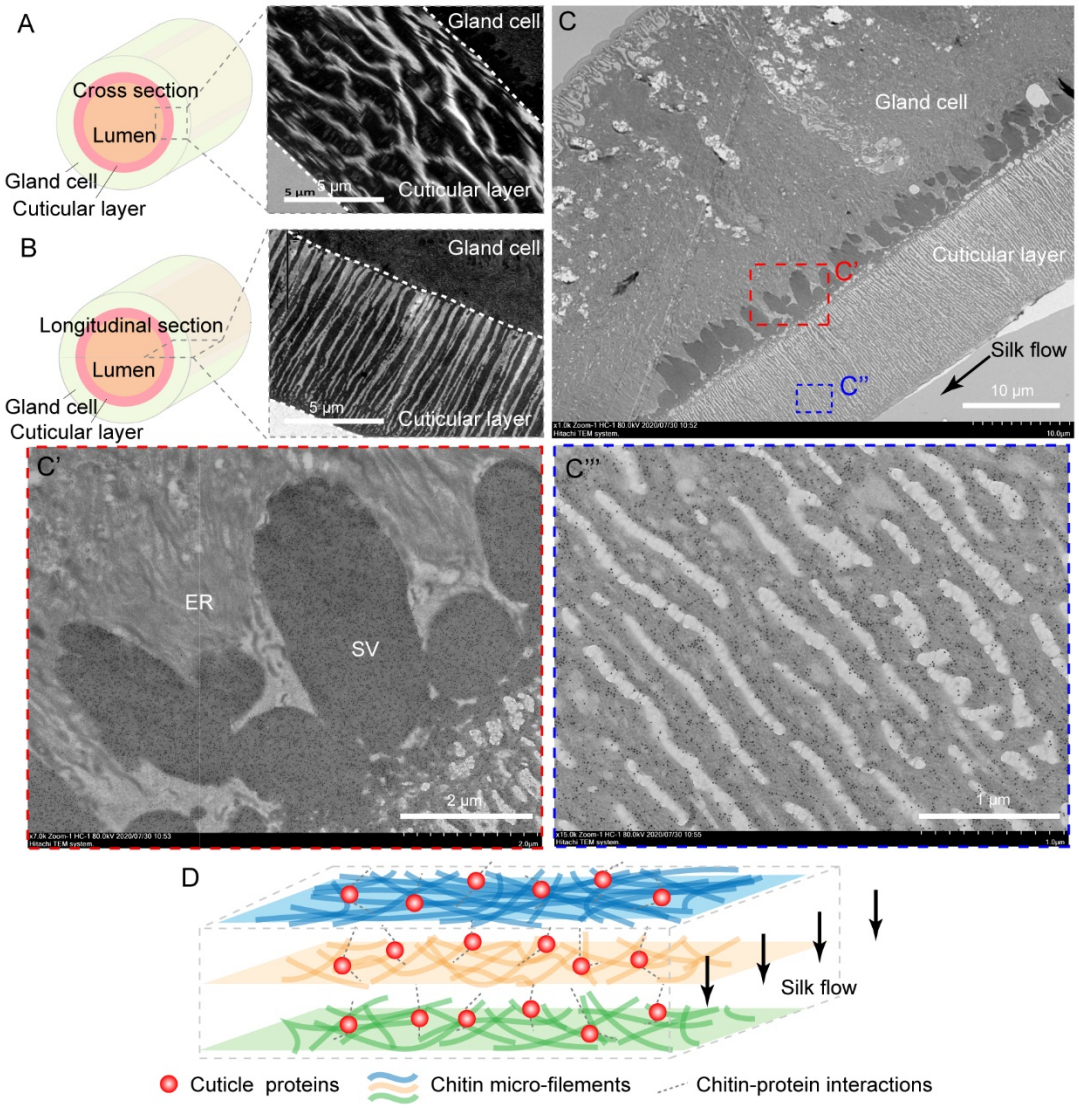

412

413 **Fig.5** Fine structure of the cuticular layer of silkworm spinning duct. **(A)** TEM images of the
414 cross-section of the cuticular layer. **(B)** TEM images of the longitudinal section of the cuticular
415 layer. **(C)** Immunoelectron microscopy shows the localization of ASSCP1 protein, which is
416 marked as black dots. Insets of C' and C'' show the distributions of ASSCP1 in the secretory
417 vesicles (C') and cuticular layer (C''), respectively. The arrow indicates the flow direction of silk
418 protein. ER, endoplasmic reticulum; SV, secretory vesicle. **(D)** Schematic illustration of the fine
419 structure of the cuticular layer.

420 **Knocking down ASSCP1 and ASSCP2 expressions affect the size of ASG**

bioRxiv preprint doi: https://doi.org/10.1101/2021.11.04.466704; this version posted November 5, 2021. The copyright holder for this preprint (which was not certified by peer review) is the author/funder, who has granted bioRxiv a license to display the preprint in perpetuity. It is made available under aCC-BY-NC-ND 4.0 International license.

and disrupt the fine structure of the cuticular layer

To investigate the functions of cuticle proteins and chitin in the spinning duct, we successfully constructed two transgenic silkworm lines (*ASSCP1*$^{-}$ *and ASSCP2*$^{-}$) in which the expression of ASSCP1 or ASSCP2 was knocked down, respectively (Figs. S5). Through cross-breeding, we obtained a transgenic line (*ASSCP1*$^{-}$*/ASSCP2*$^{-}$) that both ASSCP1 and ASSCP2 were knocked down. The economic traits of the transgenic animals from all three lines remained unchanged, and no obvious changes could be observed in the morphologies of the cocoons and pupae (Fig. S5). Molecular analysis showed that the expression of ASSCP1 or ASSCP2 was successfully knocked down from each corresponding silkworm line (Fig. S6). It can be also seen that both ASSCP1 and ASSCP2 were knocked down from the *ASSCP1*$^{-}$*/ASSCP2*$^{-}$ line (Fig. S6). The chitin content was also measured, and no significant difference was observed between the transgenic silkworm line and wild-type (*WT*) silkworms (Fig. S7). The chitin content was not changed implied that chitin synthesis and metabolism pathways were not affected after knocking down.

The most exciting finding is that knocking down the expressions of cuticle proteins affected the length of the spinning duct and the structural integrity of the cuticular layer (Fig. 6). The average lengths of the spinning duct in the *ASSCP1*$^{-}$ and *ASSCP1*$^{-}$*/ASSCP2*$^{-}$ transgenic lines decreased significantly from 23.60 mm (*WT*) to 20.75 mm and 21.05 mm, respectively (Fig. 6A and 6B). Observations showed that the decrease in length of the spinning duct in the

bioRxiv preprint doi: https://doi.org/10.1101/2021.11.04.466704; this version posted November 5, 2021. The copyright holder for this preprint (which was not certified by peer review) is the author/funder, who has granted bioRxiv a license to display the preprint in perpetuity. It is made available under aCC-BY-NC-ND 4.0 International license.

443 transgenic line resulted from smaller gland cells (Fig. 6C). The small size of the
444 gland cell did not cause any reduction in the diameter of the ASG (Fig. 6D).
445 However, the thickness of the cuticular layer decreased dramatically (Fig. 6E).
446 Knocking down the expression of ASSCP2 had a greater impact on the cuticular
447 layer than ASSCP1, and a certain synergistic effect could be found when
448 knocking down both two proteins. We further observed the ASG samples from
449 different spinning periods and measured them at different positions (anterior,
450 middle, and posterior) of the ASGs. The same results could be found (Fig. S8).
451 To have a clear view of the changes in the cuticular layer, TEM analysis
452 was performed. Compared with those from *WT* animals, the fine structure of
453 the cuticular layer from the transgenic lines was disrupted. Cross-sections of
454 the cuticular layer showed that chitin microfilaments became thinner, and gaps
455 between chitin microfilaments within lamina were compressed (Fig. 6F). As
456 listed in Table 1, the average width of the gaps decreased almost 3 times in the
457 *ASSCP1*$^{-}$*/ASSCP2*$^{-}$ transgenic line, compared with those of *WT*. Longitudinal
458 sections give more details of the changes (Fig. 6G). The average length of chitin
459 laminae dropped to ~2 μm (Table 1), suggesting that the chitin networks were
460 interrupted by the gaps. The inter-space between the chitin laminae was larger
461 in the transgenic lines, especially for *ASSCP1*$^{-}$ and *ASSCP1*$^{-}$*/ASSCP2*$^{-}$
462 transgenic lines, compared with the *WT* (Table 1). Moreover, some unidentified
463 substances filled the space between the chitin laminae. We suspect that one of
464 the unidentified substances might be the unassembled chitin because there are

bioRxiv preprint doi: https://doi.org/10.1101/2021.11.04.466704; this version posted November 5, 2021. The copyright holder for this preprint (which was not certified by peer review) is the author/funder, who has granted bioRxiv a license to display the preprint in perpetuity. It is made available under aCC-BY-NC-ND 4.0 International license.

insufficient cuticle proteins to bind to chitin.

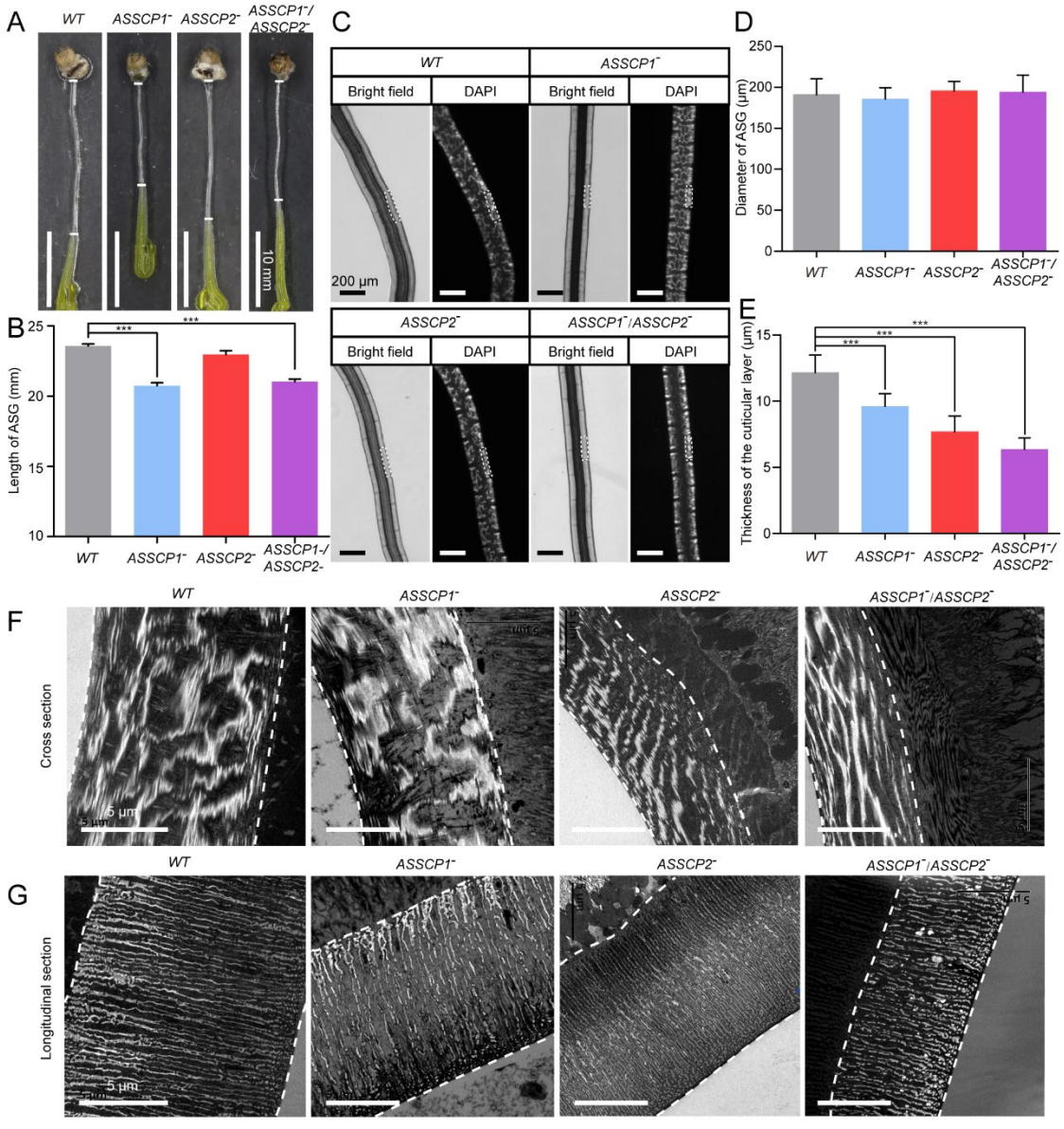

Fig. 6 Knocking down the expressions of cuticle proteins affects the length and cell size of ASG and disrupts the fine structure of the cuticular layer. **(A)** Picture of the ASG from the transgenic and *WT* animals. The narrow duct between the two white lines is the ASG. Scale bar, 10 mm. **(B)** Comparison of the length of ASG from all silkworm lines. **(C)** Cell size decreased after knocking down ASSCP1 expression. Scale bar, 200 μm. The dotted box shows the single gland cell. **(D)** Comparison of the cross-sectional diameters of ASG from all silkworm lines. **(E)** Comparison of the thickness of the cuticular layer from all silkworm lines. Scale bar, 5 μm. **(F)**

bioRxiv preprint doi: https://doi.org/10.1101/2021.11.04.466704; this version posted November 5, 2021. The copyright holder for this preprint (which was not certified by peer review) is the author/funder, who has granted bioRxiv a license to display the preprint in perpetuity. It is made available under aCC-BY-NC-ND 4.0 International license.

TEM images of the cross-section of the cuticular layer from all silkworm lines. **(G)** TEM images of the longitudinal section of the cuticular layer from all silkworm lines. Scale bar, 5 μm. ***, $p < 0.001$.

Table 1. Parameters for the structural changes of the cuticular layer after knocking down the expressions of ASSCP1 and ASSCP2.

Parameter	*WT*	*ASSCP1*$^{-}$	*ASSCP2*$^{-}$	*ASSCP1*$^{-}$/*ASSCP2*$^{-}$
Width of the gaps between chitin microfilaments in the cross section (μm)	1.77 ± 0.94	2.19 ± 1.35	0.95 ± 0.33	0.61 ± 0.17
Length of the chitin laminae (μm)	7.67 ± 1.55	2.69 ± 1.21	2.56 ± 1.12	1.73 ± 0.56
Width between adjacent chitin laminae (μm)	0.28 ± 0.09	0.59 ± 0.09	0.29 ± 0.05	0.53 ± 0.16

Knocking down the expression of cuticle protein affects silk fibrillogenesis and fiber mechanical properties

We found that the fine structure of the cuticular layer was disrupted after knocking down the expressions of ASSCP1 and ASSCP2. The relationship between the spinning duct and silk fibrillogenesis prompted us to further investigate the characteristics of silk produced by these transgenic silkworms. SEM images show that the morphologies of the cocoon surface (Fig. S9) and the single silk fiber (Fig. 7A) were similar between the transgenic and *WT* silkworms. However, the diameter of the single silk fiber from the transgenic lines slightly decreased (Fig. 7C). Further, polarized light microscopy was used to compare the mesostructures of silk fibers (Fig. 7B). The brilliant color under cross-polarized light confirmed the high orientation of all kinds of fibers. However, a deep comparison of the images in Fig. 7B shows that there were

bioRxiv preprint doi: https://doi.org/10.1101/2021.11.04.466704; this version posted November 5, 2021. The copyright holder for this preprint (which was not certified by peer review) is the author/funder, who has granted bioRxiv a license to display the preprint in perpetuity. It is made available under aCC-BY-NC-ND 4.0 International license.

492 several defects (white arrowheads) on the surface of the fiber from the
493 knocking-down silkworms, whereas only a uniform and smooth morphology
494 was observed on the surface of the *WT* silk fibers. A possible explanation of this
495 observation would be that the disruption of the fine structure of the cuticular
496 layer affected silk self-assembly and orientation during silk fiber formation.

497 We introduced FTIR analysis to quantify the content of each secondary
498 structure of silk fibers. Amide I band was used to perform the peak
499 deconvolution. Then, we determined the content of each secondary structure
500 by measuring the ratios of areas under the Gaussian peaks indicative of
501 different secondary structures (Fig. S10). Table 2 lists the content of each
502 secondary structure of silk fiber from all silkworm lines. We found that the
503 content of β-sheets decreased in the knocking down silkworm strains, while the
504 content of coils and helices, and β-turn structure increased. The results
505 obtained by morphological and structural characterizations indicate that
506 knocking down the expression of cuticle protein affects silk fibrillogenesis.

507 **Table 2.** Secondary structures of silk fibers.

Silkworm strains	β-sheets	Coils & Helices	β-turn
WT	44.99 ± 1.30	15.13 ± 0.83	9.46 ± 0.64
ASSCP1^{-}	39.36 ± 0.93^{a}	21.44 ± 0.24^{b}	18.54 ± 0.56^{c}
ASSCP2^{-}	39.28 ± 1.76	21.40 ± 0.55^{b}	18.58 ± 1.11^{c}
ASSCP1^{-}/*ASSCP2*$^{-}$	38.69 ± 0.13^{a}	21.21 ± 0.10^{b}	18.80 ± 0.10^{c}

508 a, b, and c represent the statistical differences in the corresponding secondary structures between the
509 transgenic and wild type strains (Student's *t*-test).

bioRxiv preprint doi: https://doi.org/10.1101/2021.11.04.466704; this version posted November 5, 2021. The copyright holder for this preprint (which was not certified by peer review) is the author/funder, who has granted bioRxiv a license to display the preprint in perpetuity. It is made available under aCC-BY-NC-ND 4.0 International license.

To determine whether these structural changes have negative impacts on the mechanical properties of silk fiber, we carried out tensile tests (Figs. 7D and S10). The averaged stress-strain curves of both kinds of fibers are shown in Fig. 7D, and it can be seen that the fibers from the transgenic silkworms exhibited reduced breaking stress, breaking strain, and toughness (the area of the curve). Still, a certain synergistic effect could be found when knocking down both two proteins. Comparisons of mechanical parameters such as stress, strain, Young's modulus, and toughness are also shown in Fig. 7. These data suggest that knocking down the expression of *ASSCP1* or/and *ASSCP2* had negative impacts on the mechanical properties of silk fiber, especially on silk extensibility and toughness.

bioRxiv preprint doi: https://doi.org/10.1101/2021.11.04.466704; this version posted November 5, 2021. The copyright holder for this preprint (which was not certified by peer review) is the author/funder, who has granted bioRxiv a license to display the preprint in perpetuity. It is made available under aCC-BY-NC-ND 4.0 International license.

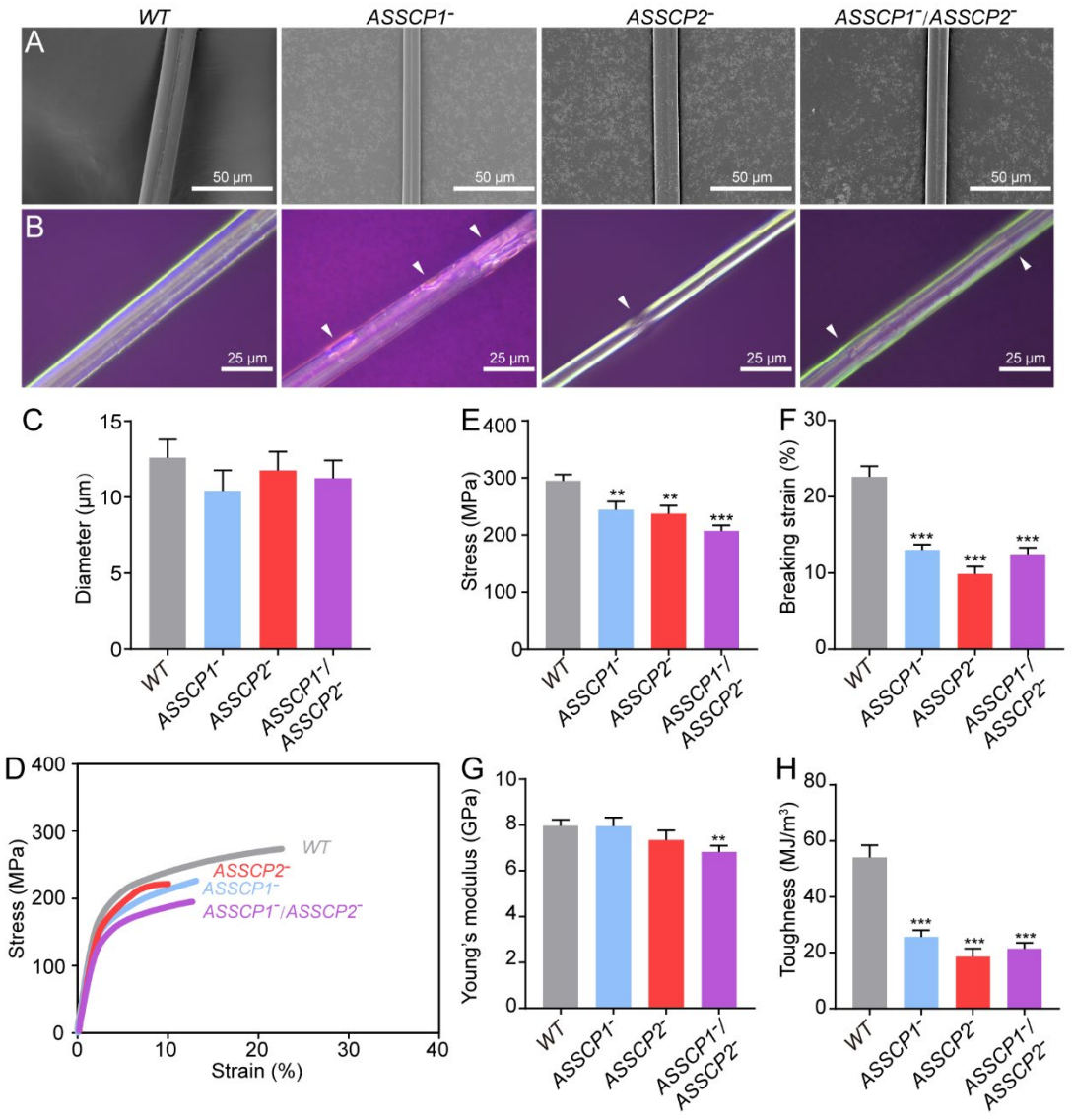

Fig. 7 Knocking down the cuticle proteins affects silk fibrillogenesis and fiber mechanical properties. **(A)** SEM images of the single silk fiber. **(B)** Polarized light microscopy images of the single silk fiber. The arrowheads indicate the defects on silk fiber. **(C)** Diameters of the single silk fibers from different strains of the silkworm. **(D)** Averaged stress-strain curves of the single silk fibers. **(E)** Breaking stress of the single silk fibers. **(F)** Breaking strain of single silk fibers. **(G)** Young's modulus of single silk fibers. **(H)** Toughness of single silk fibers. **, $p < 0.01$. ***, $p < 0.001$.

DISCUSSION

bioRxiv preprint doi: https://doi.org/10.1101/2021.11.04.466704; this version posted November 5, 2021. The copyright holder for this preprint (which was not certified by peer review) is the author/funder, who has granted bioRxiv a license to display the preprint in perpetuity. It is made available under aCC-BY-NC-ND 4.0 International license.

In this study, we identified chitin in the cuticular layer of the spinning duct of silkworms, a representative of silk-spinning arthropods. Using functional studies of the chitin-binding proteins ASSCP1 and ASSCP2, we show that chitin, ASSCP1, and ASSCP2 are the main components of the cuticular layer of the silkworm spinning duct. They participate in silk fibrillogenesis and regulate the final mechanical properties of the silk fiber.

Cuticle proteins are structural proteins, which can form the arthropod exoskeletons with chitin (Moussian, 2013). Cuticle proteins can be divided into several families, such as CPR (Karouzou et al., 2007), CPF/CPFL (Togawa, Augustine Dunn, Emmons, & Willis, 2007), CPT (Guan, Middlebrooks, Alexander, & Wasserman, 2006), CPG (Futahashi et al., 2008), CPAP1/CPAP3 (Behr & Hoch, 2005), and CPLC (Cornman & Willis, 2009). Among these families, the CPR family is the most widely distributed and found in *Lepidoptera*, *Hymenoptera*, *Coleoptera*, *Orthoptera*, *Diptera*, and *Hemiptera* (Willis & Iconomidou, 2005). The most obvious feature of the CPR family is the chitin-binding consensus, which is called the R&R consensus (Iconomidou, Willis, & Hamodrakas, 2005). The CPR family can be further divided into three types, RR-1, RR-2, and RR-3 (Andersen, 2000). Both ASSCP1 and ASSCP2 were identified as RR-2 cuticle proteins (Wang, Li, Liu, Xia, et al., 2017; Yi et al., 2013). The RR-2 consensus is rich in histidine, and the lysine residue is very conserved. These residues have been found to act as the reaction site for chitin-binding and cuticle sclerosis (Kerwin et al., 1999; Rebers & Willis, 2001). Thus,

bioRxiv preprint doi: https://doi.org/10.1101/2021.11.04.466704; this version posted November 5, 2021. The copyright holder for this preprint (which was not certified by peer review) is the author/funder, who has granted bioRxiv a license to display the preprint in perpetuity. It is made available under aCC-BY-NC-ND 4.0 International license.

552 the RR-2 type cuticle proteins are generally found in hard cuticles (Willis, 2010).
553 From our TEM pictures, it can be seen that the chitin in the cuticular layer
554 shares the same multi-layer structure as the chitin found in hard cuticles (Fig.
555 5), such as the exoskeleton (Neville, 1975). Based on this evidence, we
556 concluded that the cuticular layer, which is composed of chitin and RR-2 type
557 cuticle proteins, is hard and rigid.

558 In arthropods, chitin is present in tissues such as exoskeletons and
559 peritrophic matrix. In recent studies, chitin has also been found in spinning
560 ducts of silk-spinning arthropods such as spiders, silkworms, and caddisworms
561 (Ashton & Stewart, 2019; Davies et al., 2013). This finding suggests that silk-
562 spinning arthropods may have evolutionary homology. However, we are mainly
563 interested in why the spinning duct of arthropods needs chitin. This study
564 attempts to clarify the biological significance of chitin in the spinning duct of
565 arthropods.

566 Studies have shown that silk proteins undergo a transition from liquid to a
567 liquid crystal state in the spinning duct (Jin & Kaplan, 2003; Kerkam, Viney,
568 Kaplan, & Lombardi, 1991). When liquid silk enters the spinning duct, the shear
569 rate of the silk protein increases rapidly as the diameter of the spinning duct
570 becomes extremely small (reduced from approximately 420 μm to 80 μm)
571 (Asakura et al., 2007). The average shear rate of liquid silk fibroin is 0.1 to 0.8
572 sec^{-1} in the posterior silk gland, approximately 10^{-3} sec^{-1} in the middle silk gland,
573 and 20 to 400 sec^{-1} in the anterior silk gland (Kataoka & Uematsu, 1977).

bioRxiv preprint doi: https://doi.org/10.1101/2021.11.04.466704; this version posted November 5, 2021. The copyright holder for this preprint (which was not certified by peer review) is the author/funder, who has granted bioRxiv a license to display the preprint in perpetuity. It is made available under aCC-BY-NC-ND 4.0 International license.

574 Therefore, silk proteins bear tremendous shearing and extensional stresses
575 when they flow through the spinning duct. Shearing and extensional stresses
576 are key factors in regulating silk fibrillogenesis. A large number of studies have
577 shown that silk proteins can aggregate, self-assemble, and go through
578 fibrillogenesis under shearing and extensional stresses (Eisoldt et al., 2010;
579 Hagn et al., 2010; Holland et al., 2012; Leclerc, Lefevre, Gauthier, Gagne, &
580 Auger, 2013; Rammensee et al., 2008). These stresses in turn induce the
581 stretch and orientation of the silk molecular chains along the fiber axis (Asakura
582 et al., 2007; Vollrath & Knight, 1999). In this step, the conformational transition
583 of silk proteins from random-coil and helix-like conformations to mainly β-sheet-
584 rich structures is promoted (Vollrath & Knight, 2001). Furthermore, the silk
585 protein is converted into a solid fiber under a suitable pH gradient and metal ion
586 strength and pulled out of the spinneret by head swing (Andersson, Johansson,
587 & Rising, 2016; Sparkes & Holland, 2017; Wang, Li, Liu, Chen, et al., 2017).

588 Silk proteins have a very high shear rate when flowing through the spinning
589 duct. It is easy to see that both the silk proteins and the wall of the spinning duct
590 are subject to considerable shearing stress. The flow of the viscous silk protein
591 fluid in the lumen of the hard and rigid cuticular layer is the major source of this
592 large shear force, which promotes silk fibrillogenesis. On the other hand,
593 because the wall of the spinning duct is a single cell structure, it is the hard
594 cuticle of the inner wall of the duct lumen that bears the tremendous shearing
595 force generated by the flow to avoid the destruction of gland cells. We have

bioRxiv preprint doi: https://doi.org/10.1101/2021.11.04.466704; this version posted November 5, 2021. The copyright holder for this preprint (which was not certified by peer review) is the author/funder, who has granted bioRxiv a license to display the preprint in perpetuity. It is made available under aCC-BY-NC-ND 4.0 International license.

596 also observed a slight decrease in the thickness of the cuticular layer of the
597 spinning duct during the silk spinning process (Fig. S8), suggesting that the
598 cuticular layer may be worn down. This observation further proves this
599 hypothesis. Thus, we suggest that the biological function of chitin in the
600 cuticular layer of the spinning duct is to provide shearing stress during silk
601 fibrillogenesis and protect gland cells from shear damage.

602 Ultrastructural analysis revealed that the cuticular layer is a multilayer
603 structure by the stacking of chitin laminae (Fig. 5). The fine structure of the
604 cuticular layer is crucial for maintaining the physiological function of ASG. The
605 chitin laminae stack vertically along the duct and perpendicular to the direction
606 of silk protein transport, ensuring that the shearing force generated during the
607 flow of silk protein will not cause relative slippage between the laminae, thus
608 improving the structural stability and strength of the ASG. Further, gaps
609 between the chitin filaments within the lamina and interlayer spaces were found
610 in the cuticular layer. We have mentioned above that pH, ion strength and water
611 content also contribute to silk fibrillogenesis. Protons, metal ions and water
612 molecules are transported across the gland cells and silk proteins during silk
613 fibrillogenesis. The gaps and interlayer spaces facilitate the transportation of
614 these molecules and ensure the proper pH, ion strength, and water content for
615 silk fibrillogenesis in the ASG lumen.

616 We also found that the cuticular layer of the spinning duct is periodically
617 degraded and reformed during the molting period of silkworm larvae (Fig. 3).

bioRxiv preprint doi: https://doi.org/10.1101/2021.11.04.466704; this version posted November 5, 2021. The copyright holder for this preprint (which was not certified by peer review) is the author/funder, who has granted bioRxiv a license to display the preprint in perpetuity. It is made available under aCC-BY-NC-ND 4.0 International license.

Why does the cuticular layer need to be periodically reconstructed?

First, this phenomenon can ensure the normal growth and development of the spinning duct. The periodic reconstruction of the cuticular layer is similar to the periodic reconstruction of the arthropod exoskeleton. The exoskeleton and cuticular layer are both relatively hard. When the growth of soft and flexible tissue exceeds the support of the rigid outer matrix, degradation of the old matrix and formation of a new matrix occurs. Our observations indicate that, after the period of molting, the diameter of the silkworm spinning duct increases (Fig. S12). The duct reaches its maximum size when spinning silk, which is about twice compared with that of the 4^{th} molting.

Second, the periodic reconstruction of the cuticular layer ensures that the larvae of each instar can spin the silk fiber with good mechanical properties. In addition to spinning silk during the metamorphosis period, silkworms also spin silk at other larval developmental stages. At present, 8 kinds of silk have been identified in the silkworm larval stage (Dong et al., 2013; Peng et al., 2019). These types of silk keep the immobilized molting larvae from being blown away by heavy wind (Peng et al., 2019) and facilitate molting by anchoring their ventral feet and the old cuticle to the substratum (Hu et al., 2016).

In conclusion, this study clarified the function of chitin in the spinning duct of silk-spinning arthropods. We found that the cuticle proteins ASSCP1 and ASSCP2 are co-located and co-expressed with chitin in the cuticular layer of the spinning duct. The cuticle proteins, together with chitin, assemble in the

bioRxiv preprint doi: https://doi.org/10.1101/2021.11.04.466704; this version posted November 5, 2021. The copyright holder for this preprint (which was not certified by peer review) is the author/funder, who has granted bioRxiv a license to display the preprint in perpetuity. It is made available under aCC-BY-NC-ND 4.0 International license.

molting stage and degrades during spinning and metamorphosis. We conclude that these cuticle proteins can bind chitin and form the hard and rigid cuticular layer for supporting the cells and contributing to silk fibrillogenesis and spinning. Thus, these proteins may be the potential targets for improving the mechanical properties of silk fiber in the future. Our next works could overexpress these cuticle proteins in the spinning duct to produce high-performance silk fibers.

AUTHOR CONTRIBUTIONS

X. Wang: Conceptualization, Methodology, Writing - Original Draft, Visualization, Funding acquisition. **X. Xie:** Methodology, Formal analysis, Investigation, Visualization. **K. Xie:** Formal analysis, Investigation. **Q. Liu:** Data curation. **Y. Li:** Data curation, Writing - Review & Editing. **X. Tan:** Validation. **H. Dong:** Resources. **X. Li:** Validation. **Z. Dong:** Writing - Review & Editing. **Q. Xia:** Conceptualization, Supervision. **P. Zhao:** Writing - Review & Editing. Project administration, Funding acquisition.

ACKNOWLEDGEMENTS

This work was supported by grants from National Natural Science Foundation (Grants No. 31902216 and 31530071) and Natural Science Foundation of Chongqing, China (Grant No. cstc2020jcyj-cxttX0001).

COMPETING INTERESTS

The authors declare that they have no conflict of interest.

REFERENCES

Agrawal, S., Kelkenberg, M., Begum, K., Steinfeld, L., Williams, C. E., Kramer, K. J., . . . Merzendorfer, H. (2014). Two essential peritrophic matrix proteins mediate matrix barrier functions in the insect midgut. *Insect Biochem. Mol. Biol.,* 49, 24-34.

bioRxiv preprint doi: https://doi.org/10.1101/2021.11.04.466704; this version posted November 5, 2021. The copyright holder for this preprint (which was not certified by peer review) is the author/funder, who has granted bioRxiv a license to display the preprint in perpetuity. It is made available under aCC-BY-NC-ND 4.0 International license.

664 Andersen, S. O. (2000). Studies on proteins in post-ecdysial nymphal cuticle of locust, Locusta
665 migratoria, and cockroach, Blaberus craniifer. *Insect Biochem Mol Biol,* 30(7), 569-577.
666 Andersson, M., Johansson, J., & Rising, A. (2016). Silk Spinning in Silkworms and Spiders. *Int*
667 *J Mol Sci,* 17(8).
668 Arand, M., Friedberg, T., & Oesch, F. (1992). Colorimetric Quantitation of Trace Amounts of
669 Sodium Lauryl Sulfate in the Presence of Nucleic-Acids and Proteins. *Anal Biochem,*
670 207(1), 73-75.
671 Asakura, T., Umemura, K., Nakazawa, Y., Hirose, H., Higham, J., & Knight, D. (2007). Some
672 observations on the structure and function of the spinning apparatus in the silkworm
673 Bombyx mori. *Biomacromolecules,* 8(1), 175-181.
674 Ashton, N. N., & Stewart, R. J. (2019). Aquatic caddisworm silk is solidified by environmental
675 metal ions during the natural fiber-spinning process. *FASEB J,* 33(1), 572-583.
676 Askarieh, G., Hedhammar, M., Nordling, K., Saenz, A., Casals, C., Rising, A., . . . Knight, S. D.
677 (2010). Self-assembly of spider silk proteins is controlled by a pH-sensitive relay.
678 *Nature,* 465(7295), 236-238.
679 Behr, M., & Hoch, M. (2005). Identification of the novel evolutionary conserved obstructor
680 multigene family in invertebrates. *FEBS Lett,* 579(30), 6827-6833.
681 Chang, H., Cheng, T., Wu, Y., Hu, W., Long, R., Liu, C., . . . Xia, Q. (2015). Transcriptomic
682 Analysis of the Anterior Silk Gland in the Domestic Silkworm (Bombyx mori) - Insight
683 into the Mechanism of Silk Formation and Spinning. *PLoS One,* 10(9), e0139424.
684 Chen, C., Yang, H., Tang, B., Yang, W. J., & Jin, D. C. (2017). Identification and functional
685 analysis of chitinase 7 gene in white-backed planthopper, Sogatella furcifera. *Comp.*
686 *Biochem. Physiol. B, Biochem. Mol. Biol.,* 208-209, 19-28.
687 Cornman, R. S., & Willis, J. H. (2009). Annotation and analysis of low-complexity protein
688 families of Anopheles gambiae that are associated with cuticle. *Insect Mol Biol,* 18(5),
689 607-622.
690 Davies, G. J., Knight, D. P., & Vollrath, F. (2013). Chitin in the silk gland ducts of the spider
691 Nephila edulis and the silkworm Bombyx mori. *PLoS One,* 8(8), e73225.
692 Dong, Z., Zhao, P., Wang, C., Zhang, Y., Chen, J., Wang, X., . . . Xia, Q. (2013). Comparative
693 proteomics reveal diverse functions and dynamic changes of Bombyx mori silk proteins
694 spun from different development stages. *J Proteome Res,* 12(11), 5213-5222.
695 Eisoldt, L., Hardy, J. G., Heim, M., & Scheibel, T. R. (2010). The role of salt and shear on the
696 storage and assembly of spider silk proteins. *J Struct Biol,* 170(2), 413-419.
697 Futahashi, R., Okamoto, S., Kawasaki, H., Zhong, Y. S., Iwanaga, M., Mita, K., & Fujiwara, H.
698 (2008). Genome-wide identification of cuticular protein genes in the silkworm, Bombyx
699 mori. *Insect Biochem Mol Biol,* 38(12), 1138-1146.
700 Guan, X., Middlebrooks, B. W., Alexander, S., & Wasserman, S. A. (2006). Mutation of
701 TweedleD, a member of an unconventional cuticle protein family, alters body shape in
702 Drosophila. *Proc Natl Acad Sci U S A,* 103(45), 16794-16799.
703 Hagn, F., Eisoldt, L., Hardy, J. G., Vendrely, C., Coles, M., Scheibel, T., & Kessler, H. (2010). A
704 conserved spider silk domain acts as a molecular switch that controls fibre assembly.
705 *Nature,* 465(7295), 239-242.
706 He, B., Chu, Y., Yin, M., Müllen, K., An, C., & Shen, J. (2013). Fluorescent nanoparticle delivered
707 dsRNA toward genetic control of insect pests. *Adv. Mater. Weinheim,* 25(33), 4580-

bioRxiv preprint doi: https://doi.org/10.1101/2021.11.04.466704; this version posted November 5, 2021. The copyright holder for this preprint (which was not certified by peer review) is the author/funder, who has granted bioRxiv a license to display the preprint in perpetuity. It is made available under aCC-BY-NC-ND 4.0 International license.

4584.

Holland, C., Urbach, J. S., & Blair, D. L. (2012). Direct visualization of shear dependent silk fibrillogenesis. *Soft Matter,* 8(9), 2590-2594.

Hu, W., Liu, C., Cheng, T., Li, W., Wang, N., & Xia, Q. (2016). Histomorphometric and transcriptomic features characterize silk glands' development during the molt to intermolt transition process in silkworm. *Insect Biochem Mol Biol,* 76, 95-108.

Iconomidou, V. A., Willis, J. H., & Hamodrakas, S. J. (2005). Unique features of the structural model of 'hard' cuticle proteins: implications for chitin-protein interactions and cross-linking in cuticle. *Insect Biochem Mol Biol,* 35(6), 553-560.

Jin, H. J., & Kaplan, D. L. (2003). Mechanism of silk processing in insects and spiders. *Nature,* 424(6952), 1057-1061.

Karouzou, M. V., Spyropoulos, Y., Iconomidou, V. A., Cornman, R. S., Hamodrakas, S. J., & Willis, J. H. (2007). Drosophila cuticular proteins with the R&R Consensus: annotation and classification with a new tool for discriminating RR-1 and RR-2 sequences. *Insect Biochem Mol Biol,* 37(8), 754-760.

Kataoka, K., & Uematsu, I. (1977). On the fiber formation of silk fibroin by silkworm. *Kobunshi Ronbunshu,* 34(1), 37-41.

Kerkam, K., Viney, C., Kaplan, D., & Lombardi, S. (1991). Liquid Crystallinity of Natural Silk Secretions. *Nature,* 349(6310), 596-598.

Kerwin, J. L., Turecek, F., Xu, R., Kramer, K. J., Hopkins, T. L., Gatlin, C. L., & Yates, J. R., 3rd. (1999). Mass spectrometric analysis of catechol-histidine adducts from insect cuticle. *Anal Biochem,* 268(2), 229-237.

Khan, M. M., Morikawa, H., Gotoh, Y., Miura, M., Ming, Z., Sato, Y., & Iwasa, M. (2008). Structural characteristics and properties of Bombyx mori silk fiber obtained by different artificial forcibly silking speeds. *Int J Biol Macromol,* 42(3), 264-270.

Kramer, K. J., Hopkins, T. L., & Schaefer, J. (1995). Applications of solids NMR to the analysis of insect sclerotized structures. *Insect Biochemistry & Molecular Biology,* 25(10), 1067-1080.

Leclerc, J., Lefevre, T., Gauthier, M., Gagne, S. M., & Auger, M. (2013). Hydrodynamical properties of recombinant spider silk proteins: Effects of pH, salts and shear, and implications for the spinning process. *Biopolymers,* 99(9), 582-593.

Liu, X., Zhang, H., Li, S., Zhu, K. Y., Ma, E., & Zhang, J. (2012). Characterization of a midgut-specific chitin synthase gene (LmCHS2) responsible for biosynthesis of chitin of peritrophic matrix in Locusta migratoria. *Insect Biochem. Mol. Biol.,* 42(12), 902-910.

Liu, X., Zhang, J., & Zhu, K. Y. (2019). *Chitin in Arthropods: Biosynthesis, Modification, and Metabolism*. In Q. Yang & T. Fukamizo (Eds.), *Targeting Chitin-containing Organisms* (p. 188). Singapore: Springer, Singapore

Moussian, B. (2013). *The arthropod cuticle*. In A. Minelli, G. Boxshall & G. Fusco (Eds.), *Arthropod Biology and Evolution* (pp. 171-196). Heidelberg: Springer-Verlag Berlin

Neville, A. C. (1975). *Biology of the arthropod cuticle*. Berlin: Springer.

Noh, M. Y., Muthukrishnan, S., Kramer, K. J., & Arakane, Y. (2018). A chitinase with two catalytic domains is required for organization of the cuticular extracellular matrix of a beetle. *PLoS Genet.,* 14(3), e1007307.

Peng, Z., Yang, X., Liu, C., Dong, Z., Wang, F., Wang, X., . . . Xia, Q. (2019). Structural and

bioRxiv preprint doi: https://doi.org/10.1101/2021.11.04.466704; this version posted November 5, 2021. The copyright holder for this preprint (which was not certified by peer review) is the author/funder, who has granted bioRxiv a license to display the preprint in perpetuity. It is made available under aCC-BY-NC-ND 4.0 International license.

752 mechanical properties of silk from different instars of Bombyx mori. *Biomacromolecules,*
753 20(3), 1203-1216.
754 Pesch, Y. Y., Riedel, D., Patil, K. R., Loch, G., & Behr, M. (2016). Chitinases and Imaginal disc
755 growth factors organize the extracellular matrix formation at barrier tissues in insects.
756 *Sci Rep,* 6, 18340.
757 Rammensee, S., Slotta, U., Scheibel, T., & Bausch, A. R. (2008). Assembly mechanism of
758 recombinant spider silk proteins. *Proc Natl Acad Sci U S A,* 105(18), 6590-6595.
759 Rebers, J. E., & Willis, J. H. (2001). A conserved domain in arthropod cuticular proteins binds
760 chitin. *Insect Biochem Mol Biol,* 31(11), 1083-1093.
761 Sparkes, J., & Holland, C. (2017). Analysis of the pressure requirements for silk spinning
762 reveals a pultrusion dominated process. *Nat Commun,* 8(1), 594.
763 Su, C., Tu, G., Huang, S., Yang, Q., Shahzad, M. F., & Li, F. (2016). Genome-wide analysis of
764 chitinase genes and their varied functions in larval moult, pupation and eclosion in the
765 rice striped stem borer, Chilo suppressalis. *Insect Mol. Biol.,* 25(4), 401-412.
766 Tang, L., Liang, J., Zhan, Z., Xiang, Z., & He, N. (2010). Identification of the chitin-binding
767 proteins from the larval proteins of silkworm, Bombyx mori. *Insect Biochem Mol Biol,*
768 40(3), 228-234.
769 Togawa, T., Augustine Dunn, W., Emmons, A. C., & Willis, J. H. (2007). CPF and CPFL, two
770 related gene families encoding cuticular proteins of Anopheles gambiae and other
771 insects. *Insect Biochem Mol Biol,* 37(7), 675-688.
772 Vollrath, F., & Knight, D. P. (1999). Structure and function of the silk production pathway in the
773 spider Nephila edulis. *Int J Biol Macromol,* 24(2-3), 243-249.
774 Vollrath, F., & Knight, D. P. (2001). Liquid crystalline spinning of spider silk. *Nature,* 410(6828),
775 541-548.
776 Wang, X., Li, Y., Liu, Q., Chen, Q., Xia, Q., & Zhao, P. (2017). In vivo effects of metal ions on
777 conformation and mechanical performance of silkworm silks. *Biochim Biophys Acta,*
778 1861(3), 567-576.
779 Wang, X., Li, Y., Liu, Q., Xia, Q., & Zhao, P. (2017). Proteome profile of spinneret from the
780 silkworm, Bombyx mori. *Proteomics,* 17(12).
781 Wang, X., Li, Y., Peng, L., Chen, H., Xia, Q., & Zhao, P. (2016). Comparative transcriptome
782 analysis of Bombyx mori spinnerets and Filippi's glands suggests their role in silk fiber
783 formation. *Insect Biochem Mol Biol,* 68, 89-99.
784 Wang, X., Li, Y., Xie, K., Yi, Q., Chen, Q., Wang, X., . . . Zhao, P. (2015). Ca2+ and endoplasmic
785 reticulum Ca2+-ATPase regulate the formation of silk fibers with favorable mechanical
786 properties. *J Insect Physiol,* 73, 53-59.
787 Wang, X., Zhao, P., Li, Y., Yi, Q., Ma, S., Xie, K., . . . Xia, Q. (2015). Modifying the Mechanical
788 Properties of Silk Fiber by Genetically Disrupting the Ionic Environment for Silk
789 Formation. *Biomacromolecules,* 16(10), 3119-3125.
790 Willis, J. H. (2010). Structural cuticular proteins from arthropods: annotation, nomenclature, and
791 sequence characteristics in the genomics era. *Insect Biochem Mol Biol,* 40(3), 189-204.
792 Willis, J. H., & Iconomidou, V. A. (2005). *Cuticular Proteins*. In L. I. Gilbert, K. Latrou & S. S. Gill
793 (Eds.), *Comprehensive Molecular Insect Science* (pp. 79-109). Amsterdam: Elsevier
794 B.V.
795 Yi, Q. Y., Zhao, P., Wang, X., Zou, Y., Zhong, X. W., Wang, C., . . . Xia, Q. Y. (2013). Shotgun

bioRxiv preprint doi: https://doi.org/10.1101/2021.11.04.466704; this version posted November 5, 2021. The copyright holder for this preprint (which was not certified by peer review) is the author/funder, who has granted bioRxiv a license to display the preprint in perpetuity. It is made available under aCC-BY-NC-ND 4.0 International license.

796 proteomic analysis of the Bombyx mori anterior silk gland: An insight into the
797 biosynthetic fiber spinning process. *Proteomics,* 13(17), 2657-2663.
798 Zhang, J., & Zhu, K. Y. (2006). Characterization of a chitin synthase cDNA and its increased
799 mRNA level associated with decreased chitin synthesis in Anopheles quadrimaculatus
800 exposed to diflubenzuron. *Insect Biochem Mol Biol,* 36(9), 712-725.
801 Zhou, L., Chen, X., Shao, Z., Huang, Y., & Knight, D. P. (2005). Effect of metallic ions on silk
802 formation in the Mulberry silkworm, Bombyx mori. *J Phys Chem B,* 109(35), 16937-
803 16945.
804 Zhu, Q., Arakane, Y., Beeman, R. W., Kramer, K. J., & Muthukrishnan, S. (2008). Functional
805 specialization among insect chitinase family genes revealed by RNA interference.
806 *Proceedings of the National Academy of Sciences of the United States of America,*
807 105(18), 6650-6655.

808

809